



Research Article

Fatigue Life Evaluation of Wind Turbine Tower Based on Measured Data

Yan Zhao ^{1,2}, Xiaolu Li,³ Xinwu Wang,^{1,3} Jianqun Jiang,² and Zhenyu Wang ²

¹School of Civil Engineering, Luoyang Institute of Science and Technology, Luoyang 471023, China

²College of Civil Engineering and Architecture, Zhejiang University, Hangzhou 310058, China

³International Joint Laboratory for New Type Civil Engineering Structures of Henan Province, Luoyang Institute of Science and Technology, Luoyang 471023, China

Correspondence should be addressed to Zhenyu Wang; wzyu@zju.edu.cn

Received 8 February 2023; Revised 30 June 2023; Accepted 20 July 2023; Published 19 August 2023

Academic Editor: Xiao Sun

Copyright © 2023 Yan Zhao et al. This is an open access article distributed under the Creative Commons Attribution License, which permits unrestricted use, distribution, and reproduction in any medium, provided the original work is properly cited.

Fatigue life is a crucial design factor which dictates the safe operation of the wind turbines, but it is influenced by uncertain factors such as environmental loads, analytical models, material properties, and manufacturing methods. In this study, a 1.5 MW wind turbine was monitored in operation to understand the fatigue mechanism and enhance wind turbine design. The influence of different operating conditions on fatigue damage was analyzed by correlating strain monitoring data with supervisory control and data acquisition (SCADA) data. Furthermore, a fatigue evaluation method based on measured strain data was proposed. Fatigue damage increases with the increase of wind and rotation speed. More than 50% of the damage occurred at the rated rotation speed state, the corresponding wind speed was greater than the rated wind speed and the pitch control system was active. The findings of this study provide insights for investigating the real fatigue state of similar wind turbine towers and improving the return on investment by closely estimating their service life.

1. Introduction

Wind power has maintained its position as the fastest growing renewable energy source worldwide in the past 20 years [1]. While there have been considerable advances in wind power technology, there are also some challenges, such as the increasing of installed capacity and scale of wind turbines, they are more sensitive to dynamic loads, and vulnerability to fatigue damage. Therefore, it is crucial to accurately predict the actual fatigue damage of wind turbine structures, especially fatigue performance of the welded joints.

Researchers have conducted extensive investigations on fatigue assessment of the wind turbine structures. Repetto and Solari [2–5] explored the dynamic response and wind-induced fatigue of a highly flexible structure under wind load and proposed a method for calculating the fatigue life. However, they did not consider the distribution of wind speed and direction during fatigue analysis. Tempel [6] used the frequency domain method to evaluate the fatigue life of the supporting structure of a monopile offshore wind turbine and revealed that aerodynamic

damping had a strong influence on dynamics of the supporting structure. Hence, it is crucial to accurately determine the magnitude of aerodynamic damping. Bagbanci et al. [7] considered the influence of environmental factors such as wind, wave, and current on the design load of a monopile offshore wind turbine structure during fatigue assessment. Kvittem and Moan [8] assessed the sensitivity of necessary simulation duration and environmental conditions to the long-term fatigue damage of a 5 MW wind turbine and showed that the turbine experienced high-fatigue damage when it was in resonance. Hence, it is necessary to optimize the dynamic characteristics of the wind turbine to avoid rapid increase in fatigue damage of the supporting structure. Stavridou et al. [9] demonstrated that circumferential welds between tower subparts and between the tower and connecting flanges were susceptible to the fatigue damage. The fatigue of two towers with the same height and different thickness distributions was investigated using the numerical and analytical methods, and the results showed that the thickness of the tower was a decisive factor of the fatigue life.

All these studies were based on the numerical models. However, the accuracy of stress time history considerably influences the fatigue evaluation results. A small change in the stress range can produce significantly different fatigue assessment results because the fatigue life is at least inversely proportional to the third power of the stress range [10–12]. At the same time, considering all influencing factors in the traditional simulation analysis is time consuming. By installing sensors on the structural unit, measuring and recording the actual stress of the structure can provide reliable data for fatigue assessment, accurately estimate the actual damage state of the structure, and reduce the periodic inspection of the structure to a certain extent [13, 14].

The studies on fatigue assessment of the wind turbine structure based on long-term monitoring data are limited. Pollino and Huckelbridge [15] used strain gauges to monitor a 100 kW wind turbine for approximately 1 year and concluded that the fatigue life of the wind turbine support structure was significantly higher than 20 years. Weijtens et al. [16] measured the loads of two 3 MW wind turbines in the Northwind offshore wind farm and analyzed the relationship between environmental and operation conditions and fatigue damage. Loraux [17] monitored the structural vibration of a Vestas V90–2.0 MW wind turbine in Switzerland for 3 years, they combined the monitoring data with supervisory control and data acquisition (SCADA) data to evaluate the fatigue safety of the tower and provide a realistic estimate of fatigue duration. Mai et al. [18] used measured strain to link the oceanographic data with the fatigue damage, and the Bayesian method was used to update the joint distribution of the oceanographic data. Consequently, the remaining fatigue life of the support structure can be updated, and eventually provide decision support for the operation of wind turbines. These monitoring activities enable more accurate structural engineering methods for the safety verification of wind turbine structures. However, different environments and structural types have varied effects on fatigue damage, thus, more wind fields should be monitored to obtain a better understanding of the relationship between fatigue damage and operational factors. In addition to the wind turbine support structures, studies on the fatigue assessment and residual life prediction of steel structure bridges based on field measurement can be used for reference. Xu et al. [19] analyzed the wind-induced fatigue of Qingma bridge. Joint probability density function of wind speed and direction was established according to data collected by the monitoring system. Then, the stress characteristics of the hot spot under different wind speeds and directions were analyzed using the finite element model, the fatigue damage model based on continuous damage mechanics was used to calculate the fatigue damage at the hot spot. Ni et al. [20] and Ye [11] monitored the dynamic strain of Qingma bridge for a long time. Considering the similarity of stress spectrum characteristics under normal traffic and wind conditions and the differences during typhoon weather, the standard daily stress spectrum considering the influence of traffic load and typhoon weather was established, and thus the fatigue life of Qingma bridge was evaluated via Miner's linear cumulative damage method.

In this study, the fatigue life of a wind turbine tower structure was evaluated using long-term SCADA and strain monitoring data. First, wind speed, wind direction, rotation speed, and blade pitch angle of the wind turbine were statistically analyzed, according to which the operating conditions of the wind turbine were divided into seven categories. Second, rainflow counting algorithm was used to convert the stress time history into stress spectrum, and the hourly fatigue damage throughout the monitoring period was calculated based on the Palmgren–Miner damage accumulation rule. The influence of wind speed, rotation speed, and blade pitch angle on fatigue damage was also analyzed. Finally, the maximum and average hourly damage matrices were established according to the joint probability distribution of wind speed and direction, and fatigue life was analyzed.

This paper is organized as follows: Section 2 gives the basic theory of fatigue damage calculation for the wind turbine tower, including S–N curve, extrapolation of hot spot stress, mean stress correction model, and Palmgreen–Miner linear accumulation rule. Section 3 describes the turbine and the monitoring plan. Making use of the monitoring data, Section 4 summarizes the operational and environmental conditions of the monitoring wind turbine, and categorizes the operating states. The variation of measured stress data with average wind speed is also analyzed and discussed. Section 5 proposes a fatigue life assessment process based on monitoring data. First, Section 5.1 determines the stress concentration factor (SCF) at the weld near the sensor based on a refined local finite element model. Section 5.2 discusses the influence of environment/operation conditions on fatigue damage. Section 5.3 provides the fatigue life assessment process and constructs a damage matrices in Section 5.4. Section 5.5 evaluates the fatigue life of the wind turbine tower. Finally, the main conclusions are summarized in Section 6.

2. Fatigue Calculation Method

2.1. S–N Curve. The fatigue resistance of structures is typically illustrated by the S–N curve, it was determined via a series of fatigue tests on specimens. Parameters of S–N curve are different in the fatigue assessment due to diverse structural forms and material properties. International wind turbine design standards International Electrotechnical Commission (IEC) [21] and Det Norske Veritas and Germanischer Lloyd (DNVGL) [22] provide guidance for the calculation of fatigue life. As presented in DNVGL [22], different S–N curves are used to evaluate the fatigue capacity of various welded joints in wind turbines. The S–N curve is expressed as follows:

$$\log N = \log a - m \log \left(\Delta \sigma \left(\frac{t}{t_{ref}} \right)^k \right), \quad (1)$$

where $\Delta \sigma$ is the stress range; N is the predicted number of cycles corresponding to fatigue failure for the stress range $\Delta \sigma$; m is the negative inverse slope of the S–N curve in the double-logarithmic coordinate; $\log a$ is the intercept on the $\log N$ axis; t is the thickness through which a crack will most

likely grow; t_{ref} is the reference thickness; and k is the thickness exponent on fatigue strength.

In this study, the D -type bilinear S - N curve was used for the fatigue calculations. If the structure conforms to the S - N curve recommended by other standards, then these standards can also be used if the S - N curve comprehensively considers the contribution of all related damage.

2.2. Extrapolation of Hot Spot Stress. The flange of the wind turbine is welded by the large diameter cylinder wall and flange plate, which is a typical plate weld. For the fatigue life evaluation of welded structures, the hot spot stress analysis shall be carried out, and take the hot spot stress range at the position where fatigue failure is most likely to occur as the design basis [23]. However, it is impossible to measure the hot spot stress at the flange weld, and only the nominal stress at a certain distance from the weld toe can be measured because of limitations of sensor installation conditions [12]. Therefore, it is crucial to calculate the SCF at the weld between the tower and flange plate and convert the measured nominal stress to the hot spot stress at the weld.

The stress concentration at the weld toe is generally assumed to be composed of two parts, namely, structural stress concentration caused by geometric discontinuity between the entire structure and the joint, and stress concentration caused by notches (such as defects, cracks, notches, etc.) of the weld itself. When the hot spot stress method is used, only the structural stress concentration needs to be considered, the notch effect due to the weld is included in the S - N curve [22, 24].

Determining the actual value of hot spot stress at the weld toe is difficult because of the complex configuration and stress states at welded joints. It can be estimated by extrapolating the stress at adjacent points far from the weld. The calculation methods are as follows:

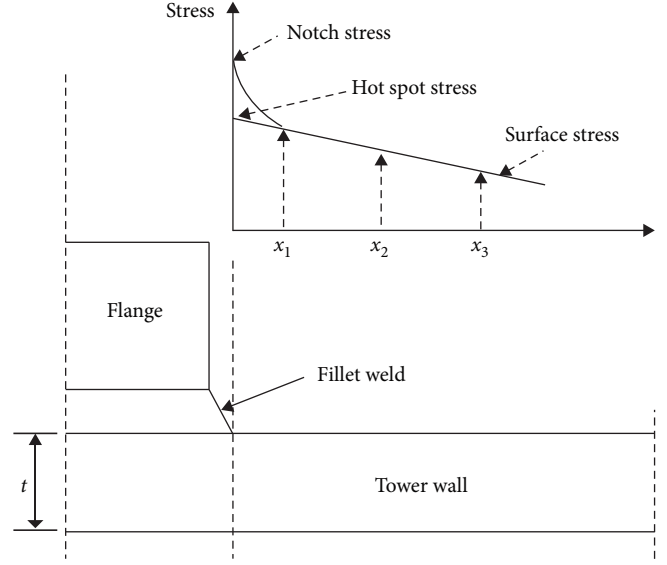


FIGURE 1: Calculation principle of surface extrapolation method [22].

Fixed-point method:

$$\sigma_h = 1.12\sigma_{0.5t}. \quad (2)$$

Linear extrapolation method:

$$\sigma_h = \frac{x_2\sigma_s(x_1) - x_1\sigma_s(x_2)}{x_2 - x_1}. \quad (3)$$

Quadratic extrapolation method:

$$\sigma_h = \frac{x_2x_3(x_3 - x_2)\sigma_s(x_1) + x_1x_3(x_1 - x_3)\sigma_s(x_2) + x_1x_2(x_2 - x_1)\sigma_s(x_3)}{x_2x_3(x_3 - x_2) + x_1x_3(x_1 - x_3) + x_1x_2(x_2 - x_1)}, \quad (4)$$

where σ_h is the hot spot stress value at the weld toe; x_1, x_2, x_3 are extracting points at a certain distance from the weld toe, as shown in Figure 1; $\sigma_s(x_1), \sigma_s(x_2), \sigma_s(x_3)$ are the structural stress values at the extracting points x_1, x_2, x_3 , respectively.

When the surface extrapolation method is used to calculate the hot spot stress, identifying appropriate extracting points is crucial. These extracting points must, theoretically, be outside the influence area of the notch effect but sufficiently close to the weld toe to ensure that the stress concentration arising from the structure can be captured [22]. In plate or shell structures, typically, hot spots are of three types: (a) weld toe located on the plate surface at an ending attachment, (b) weld toe around the plate edge of an ending attachment, and (c) weld toes on both the mother plate and the attachment surface. The flange weld belongs to the "c" type hot spot, and the influence area of the stress concentration near the hot spot is generally less than $0.5t$ (where t is the plate thickness). Beyond this area, stress change on the plate

surface is stable [22]. DNVGL and International Institute of Welding (IIW) both provide the location of extracting points for the surface extrapolation method [22, 23].

2.3. Correction of Mean Stress. The mean value of the stress cycle is ignored in many cases of fatigue analysis of wind turbine support structures. High-mean stress corresponds to serious fatigue damage and short fatigue life at the same stress range. Therefore, many mean stress correction models, including Gerber, Goodman, and Soderberg models, have been proposed [25, 26]. Among them, the Goodman model is the most commonly used and expressed as follows:

$$\Delta\sigma' = \frac{\Delta\sigma}{1 - \frac{\sigma_m}{\sigma_t}}, \quad (5)$$

where $\Delta\sigma$ is the stress range at non-zero mean stress σ_m ; $\Delta\sigma'$ is the equivalent stress range at zero mean stress; σ_m is the mean stress, and σ_t is the ultimate tensile strength of steel.

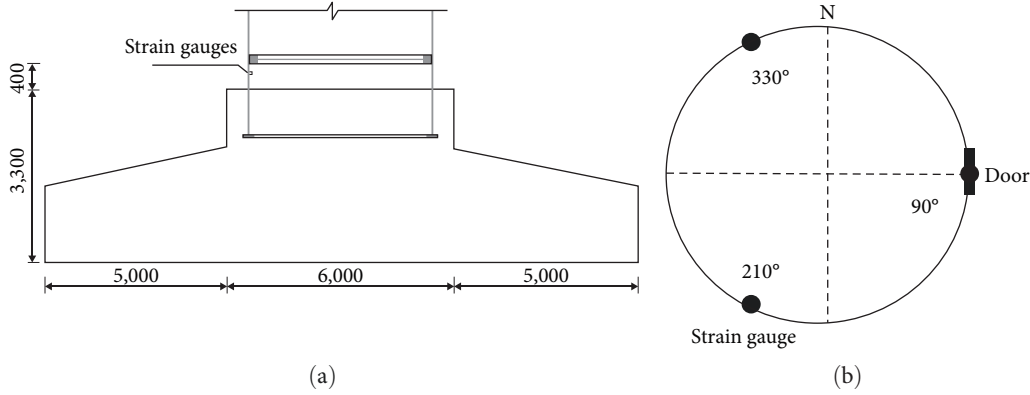


FIGURE 2: Installation position of strain gauge. (a) Installation height of strain gauge (unit: mm). (b) Installation orientation of strain gauge.

2.4. Fatigue Damage Accumulation. Stress time history comprises many stress pulses because of the randomness and dynamic characteristics of loads acting on wind turbines. Rainflow counting algorithm is necessary to ease the calculation burden and simplify the complex and irregular measured stress time history into the stress spectrum, which can reflect the real situation. The stress spectrum consists of two elements, namely, stress range (S) and its corresponding number of cycles (N).

The number of cycles corresponding to different stress amplitudes can be calculated after the rainflow algorithm is applied to the stress time history. According to the Palmgren–Miner damage accumulation rule, for a series of stress ranges $\Delta\sigma_1, \Delta\sigma_2, \Delta\sigma_3, \dots$, the number of cycles to failure is N_1, N_2, N_3, \dots , and the actual number of cycles is n_1, n_2, n_3, \dots . The damage component D_i is calculated as the actual number of cycles for each stress amplitude divided by the number of cycles at which fatigue failure occurred under that stress amplitude. Damage components generated by each cyclic load are assumed independent of each other, and the accumulated fatigue damage D is the linear superposition of damage components generated by each cyclic load and expressed as follows [22]:

$$D = D_1 + D_2 + D_3 + \dots = \frac{n_1}{N_1} + \frac{n_2}{N_2} + \frac{n_3}{N_3} + \dots = \sum_i \frac{n_i}{N_i}, \quad (6)$$

where n_i is the actual number of cycles under the i -th level stress range; N_i is the allowable number of cycles when fatigue failure occurs under the i -th level stress range, which can be determined from the S–N curve; i is the total number of stress ranges corresponding to all operating conditions involved in the fatigue calculation.

3. Monitoring Plan

The rated power of the wind turbine is 1.5 MW and the hub height is 70 m in this study. Cut-in and cutout wind speeds ($V_{\text{cut-in}}$ and V_{cutout}) of the wind turbine are 3 and 22 m/s (average wind speed of 10 min), respectively, and the rated wind speed (V_{rated}) is 11 m/s. The rated rotation speed of the

wind turbine is 17.3 rpm, and the grid-connected rotation speed is 9 rpm. Power generation increases gradually when the wind speed changes from $V_{\text{cut-in}}$ to V_{rated} . Power is stable at around 1.5 MW when the wind speed is greater than V_{rated} . Blades will be feathered to avoid damage caused by excessive wind load when the 10 min mean wind speed exceeds V_{cutout} .

Modern wind turbines are typically equipped with a SCADA system. It comprises a microprocessor and several sensors, and remotely connected to the main control room, which is used to control the operation and monitor the performance of the wind turbine. The SCADA system collects and records the operation data of the wind turbine, including wind speed, wind direction, rotation speed, nacelle azimuth, generator speed, blade pitch angle, and power generation, at a specific sampling frequency (1/7 Hz in this study) during the monitoring period. These data are used by the control system to manage the operations of the turbine, such as startup and shutdown of rotor, emergency shutdown, adjustment of nacelle azimuth, and blade pitch angle.

Three vertical strain gauges are arranged on the inner wall of the foundation ring of the wind turbine. These strain gauges are installed 100 mm downward from the flange. Strain data were measured at 90°, 210°, and 330°, as shown in Figure 2. However, the strain gauge at 90° was damaged, and these data are unavailable. In addition, measured strain data were simply caused by the external wind load because the strain gauge was installed 2 years after the normal operation of the wind turbine.

4. Analysis of Monitoring Data

4.1. Statistics and Classification of Operating Conditions. The wind turbine presents different characteristics in various operating states. Understanding statistical characteristics of wind turbine operation and wind conditions using SCADA data and reasonably classifying its operating conditions is crucial to master the influence of wind speed, rotation speed, and blade pitch angle on fatigue damage. Therefore, operation parameters, such as wind speed, rotation speed, blade pitch angle, and nacelle azimuth angle, were statistically analyzed in this section using SCADA data of the monitoring wind turbine.

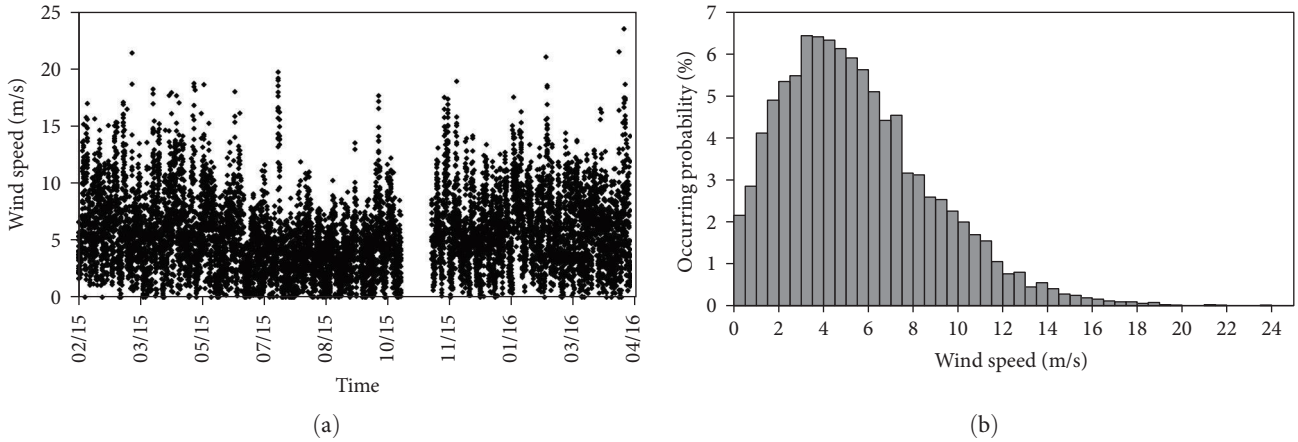


FIGURE 3: Variations of wind speed and corresponding statistical analysis during monitoring period. (a) Monitoring data of wind speed. (b) Occurrence probability of wind speed.

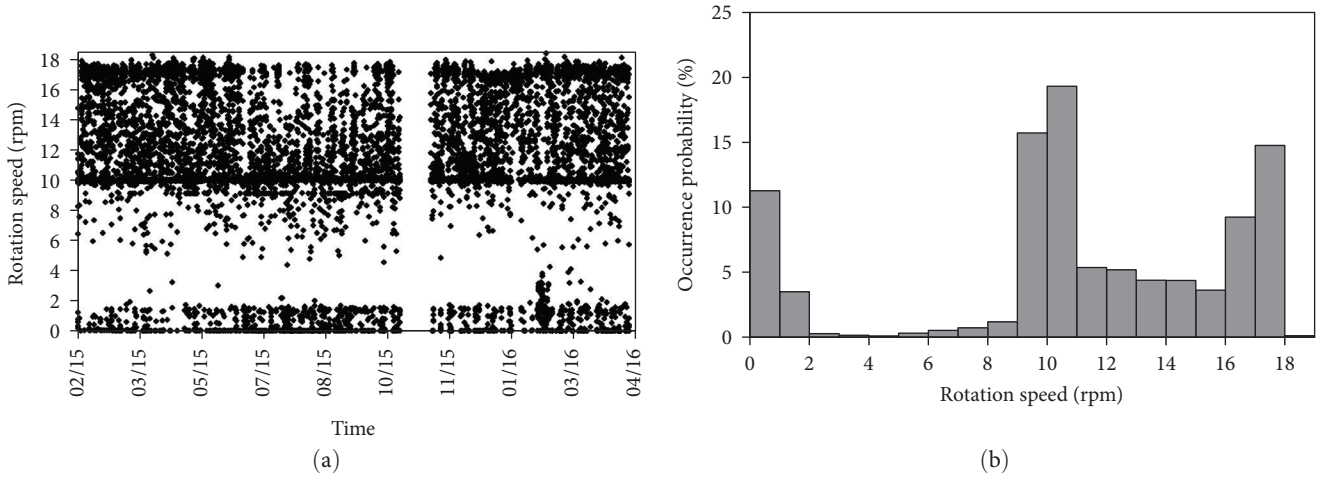


FIGURE 4: Variations of rotation speed and corresponding statistical analysis during monitoring period. (a) Monitoring data of rotation speed. (b) Occurrence probability of rotation speed.

Figures 3–6 statistically present the wind speed, rotation speed, blade pitch angle, and nacelle azimuth angle. As shown in Figure 3, the wind speed varied in the range of 0–23.52 m/s, mainly in the range of 2–8 m/s. As shown in Figure 4, the maximum rotation speed of the rotor was 18.38 rpm, about 30.42% of rotation speed was in the range of 9.5–10.5 rpm, while 24% reached the rated speed of 17.3 rpm. As shown in Figure 5, the probability of the pitch angle in the range of 0°–20° was 78%. The pitch angle of the blade was 0° when the wind speed was less than V_{rated} , which helped in maximizing the windward area of the rotor and generate more energy. The pitch angle of the blade was adjusted in the range of 0°–20° when the wind speed was greater than V_{rated} to maintain the rotation speed at the rated rotation speed. The probability of the pitch angle near 88° was 4.45%, and the wind turbine was in shutdown state with the blades were feathered. After the shutdown program was completed without fault, the turbine entered the standby state, so that the turbine can be put into operation and generate power quickly when the wind speed was greater than

3 m/s. The pitch angle at standby state was around 50°, and its occurrence probability was 16.3%. The wind speed corresponding to both the shutdown and standby states of the turbine was less than V_{cut-in} . The nacelle rotated around the tower axis with the wind direction when the wind turbine was operational to align with the wind direction, obtaining the maximum wind energy. Therefore, as shown in Figure 6, the nacelle azimuth angle changes with the wind direction in the range of 0°–360°. The probability of the nacelle azimuth angles around –20°–20° and 220°–260° was higher than that of other azimuth angles, with the former being the main wind direction (MWD) and the latter being the secondary wind direction (SWD).

The operation state of the wind turbine studied in this paper was then divided into seven load cases (LCs) according to operational characteristics in Figures 3–6, as presented in Table 1 [27]. The values presented in bold in Table 1 are prerequisite for every operational state, while values with normal font represent the range of operational parameters under these LCs.

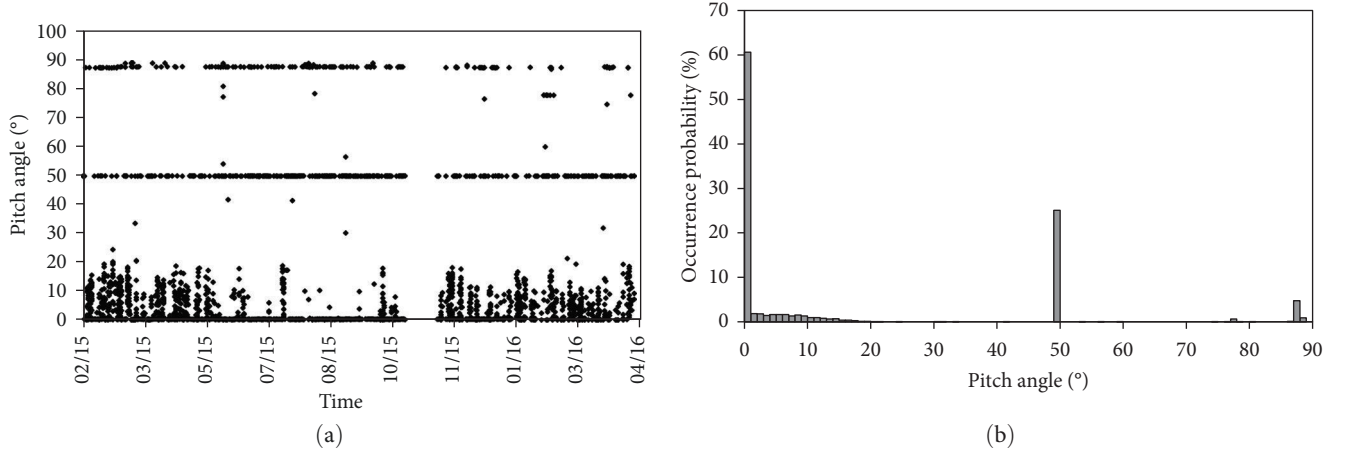


FIGURE 5: Variations of pitch angle and corresponding statistical analysis during monitoring period. (a) Monitoring data of pitch angle. (b) Occurrence probability of pitch angle.

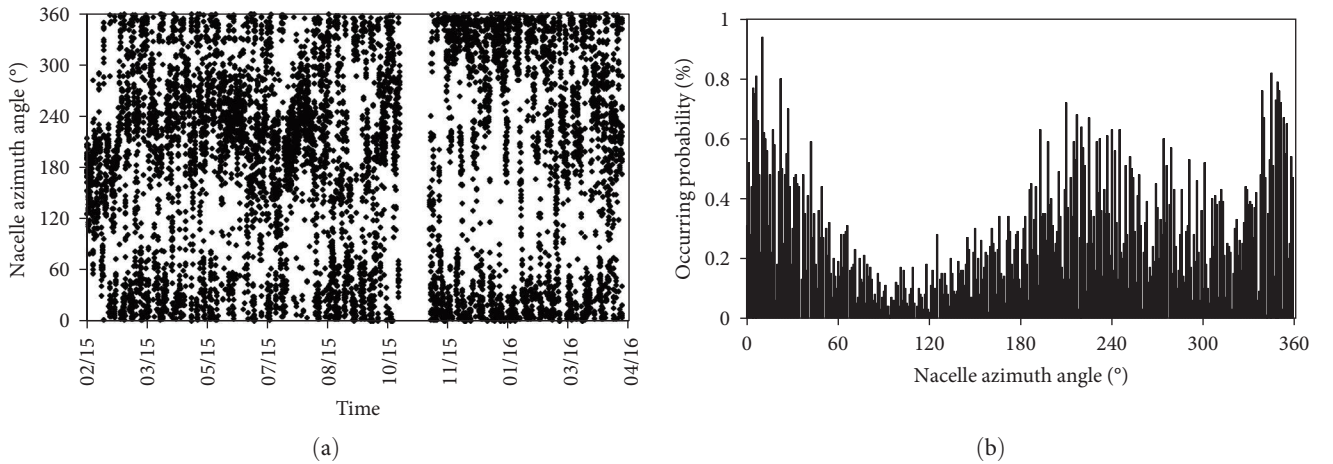


FIGURE 6: Variations of nacelle azimuth angle and corresponding statistical analysis during monitoring period. (a) Monitoring data of nacelle azimuth angle. (b) Occurrence probability of nacelle azimuth angle.

TABLE 1: Definition of operational states for wind turbines.

LC	Operational state	Wind speed (m/s)	Rotation speed (rpm)	Pitch angle ($^{\circ}$)
LC 1	Shutdown	0–22	0–3	75–90
LC 2	Standby	0–10	0–3	49–50
LC 3	Transition of startup and shutdown	0–3	2–9	± 0
LC 4	Grid-connected rotation speed	1–6	9–10.5	± 0
LC 5	Medium rotation speed	3–9	10.5–16	± 0
LC 6	Rated rotation speed	11	16–18.38	0–20
LC 7	Cutout wind speed	>22	0–4	75–90

LC 1 was the shutdown state. At this time, the pitch angle was in the range of 75° – 90° , the rotation speed was 0–3 rpm, and the wind turbine was in the idling state. Due to the possibility of shutdown in many cases, such as manual shutdown and troubleshooting, the corresponding wind speed range was relatively wide.

The wind turbine entered the standby state (LC 2) after the shutdown program was completed successfully and there is no fault. At this time, the wind turbine operated at a slow

rotation speed and had no power output. The rotation speed varied freely from 0 to 3 rpm, the pitch angle was around 50° , and the rotor brake was released so that wind turbine can be put into operation and generate power quickly when the wind speed was greater than 3 m/s.

LC 3 was the transition condition of startup and shutdown, which referred to the startup process of wind turbine from standby state (LC 2) to grid-connected power generation, or the shutdown process from grid-connected power

generation to shutdown state (LC 1). The rotation speed and wind speed were in the range of 2–9 rpm and 0–4 m/s, respectively. The pitch angle was around 0° so that the windward area of blades was maximized and the most wind energy was obtained.

LC 4 was the grid-connected rotation speed condition. The rotation speed of wind turbine will increase gradually after the startup process. When power generation of wind turbine was integrated into electricity grid, the corresponding rotation speed was called grid-connected rotation speed. When the turbine shut down, the rotation speed gradually decreased and also passed through the grid-connection rotation speed. The rotation speed corresponding to this operational state was within the range of 9–10.5 rpm. To ensure the maximum windward area of the blades, the pitch angle was always maintained around 0° .

LC 5 was the medium rotation speed condition, where the range of corresponding rotation speed was 10.5–16 rpm. At this time, the wind speed was lower than the rated wind speed (11 m/s), and the rotation speed was lower than the rated rotation speed too. The blade pitch angle was around 0° to ensure the maximum utilization of wind energy.

When the wind speed was greater than V_{rated} , the rotation speed reached the rated rotation speed of 17.3 rpm and then stabilized around this value, which was the rated rotation speed state (LC 6). Under this operational state, the pitch angle increased from 0° to 20° with the increase of wind speed to adjust the windward area of the rotor, ensure that a constant load acted on the rotor, maintain the rotation speed close to the rated rotation speed, and ensure the maximum electric energy output.

LC 7 was the cutout wind speed condition. At this time, the average wind speed in 10 min was greater than 22 m/s, the wind turbine entered a feathered shutdown state. The pitch angle was around 90° , the rotation speed was 0–4 rpm. The wind turbine will idle to avoid potential damage of the structure caused by excessive wind load.

The relationship between different operational parameters and fatigue damage of the wind turbine are discussed in detail on the basis of these seven LCs.

4.2. Stress Monitoring. Measured strain data were considered to be caused only by the external wind load because the strain gauges on the tower bottom foundation ring were installed 2 years after the wind turbine became operational. The pressure stress at the bottom of the tower caused by self-weight of the wind turbine was approximately 5.8 MPa, and the stress caused by the eccentricity of the rotor was approximately 1.8 MPa.

Figure 7 shows how the measured stress data changed with average wind speed during the monitoring period. Points of various colors in Figure 7 corresponding to different operation states were summarized in Table 1. The stress at the tower bottom in the fore–aft (FA) direction first increased and then stabilized with the increase of the average wind speed. In the range of 0–4 m/s (including LCs 1–3), the measured stress was highly discrete. This was because the wind speed was near the cut-in wind speed, and the wind

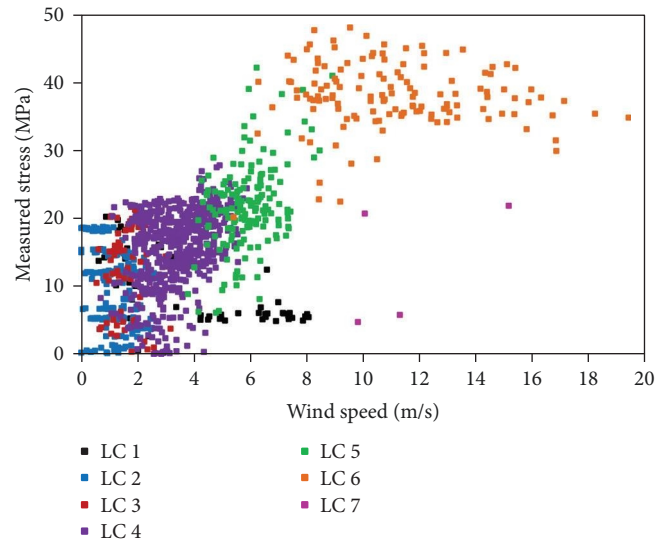


FIGURE 7: Relationship between measured stress of tower bottom and average wind speed.

turbine was affected by the startup and shutdown of the rotor and yaw motion, etc. The stress at the tower bottom reached the maximum value of 48.13 MPa at the rated wind speed of 11 m/s. When the wind speed was higher than V_{rated} , the stress at the tower bottom was stable in the range of 33–48 MPa. This was because the pitch control system was active, and the pitch angle was adjusted in the range of 0° – 20° when the wind speed was higher than V_{rated} to ensure the stability of wind load on the rotor. Points of different colors in Figure 7 corresponding to different operation states were summarized in Table 1.

5. Fatigue Life Assessment Based on Monitoring Data

5.1. Calculation of Stress Concentration Factor. For several typical welded joints, researchers have used different finite element software programs, simulation methods, element types, and mesh sizes to perform the comprehensive comparative analyses of theoretical and measured values of the hot spot stress and fatigue test results of local and global models. They have also presented suggestions for the finite element calculation method based on surface extrapolation [24, 28].

As shown in Figure 8, a half structure model of the foundation and tower was established according to the symmetrical relation of structure and load, and a symmetrical boundary was added on the symmetrical surface of the structure. The tower and foundation ring flange made of Q345 steel had a yield strength of 345 MPa, elastic modulus of 210 GPa, and Poisson's ratio of 0.3. The foundation and tower extended outward to a certain length, which helped to eliminate the influence of the loading point at an upper location and the consolidation boundary at a lower location on the flange stress. A reference point (Figure 8) was created at the center of the upper end face of the tower. All nodes on the upper end face of the tower wall were coupled with full

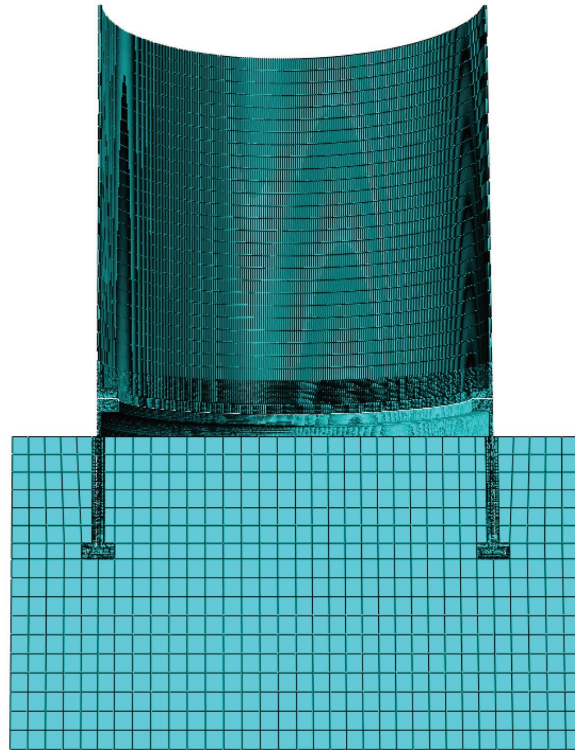


FIGURE 8: Half structure model of the foundation and tower.



FIGURE 9: Maximum principal stress diagram of flange (unit: MPa).

degrees of freedom of the reference point, and the bending moment was directly applied to the reference point and transmitted to the tower and foundation. Ties were used to connect upper and lower flange plates as well as the lower end of the tower wall and the top of the foundation ring. The top surface of the foundation ring and the lower flange plate was the main surface, and the bottom surface of the lower tower wall and the upper flange plate was the secondary surface. Normal behavior of the contact surface was hard contact, tangential behavior was defined as Coulomb friction, and the friction coefficient was 0.35. The contact effect between the foundation ring and concrete was considered, and the friction coefficient was set to 0.4. The shell element (S4R) was used to mesh the tower and foundation ring, and the solid element (C3D4) was used to simulate the concrete. The mesh was refined around the weld, and the results of

different mesh precision values were compared to eliminate the calculation errors caused by the mesh size.

Normal operation load of the wind turbine was used for analysis. The vertical force was $-2,648.8$ kN, horizontal force was 358.2 kN, bending moment was $22,868$ kN-m, and torque was 373.9 kN-m. The hot spot stress near the flange weld was obtained via the finite element method, as shown in Figure 9.

The following SCF K_{SCF} was calculated using the stress value at the location where the strain sensor was installed (100 mm downward from the flange) as the reference stress:

$$K_{SCF} = \frac{\sigma_h}{\sigma_r}, \tag{7}$$

where σ_h is the hot spot stress and σ_r is the reference stress. The hot spot stress and corresponding SCF K_{SCF} at the weld

TABLE 2: Stress concentration factor K_{SCF} .

Extrapolation method	Normal operating condition		Extreme load condition	
	σ_h (MPa)	K_{SCF}	σ_h (MPa)	K_{SCF}
Fixed-point method	78.42	1.25	168.25	1.21
Linear extrapolation method	70.52	1.12	150.65	1.08
Quadratic extrapolation method	69.75	1.11	149.07	1.07

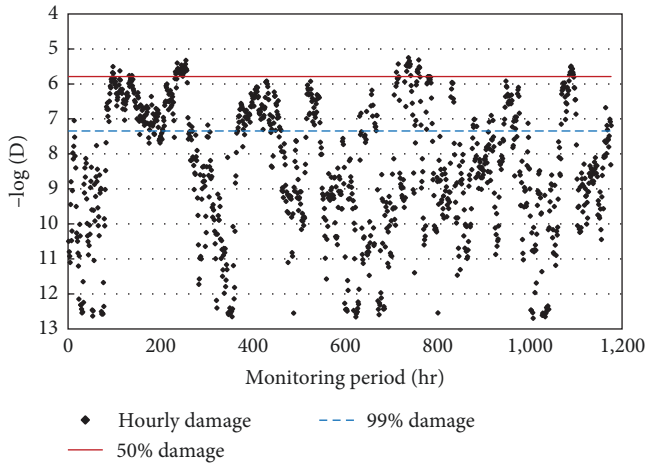


FIGURE 10: Hourly fatigue damage during monitoring period.

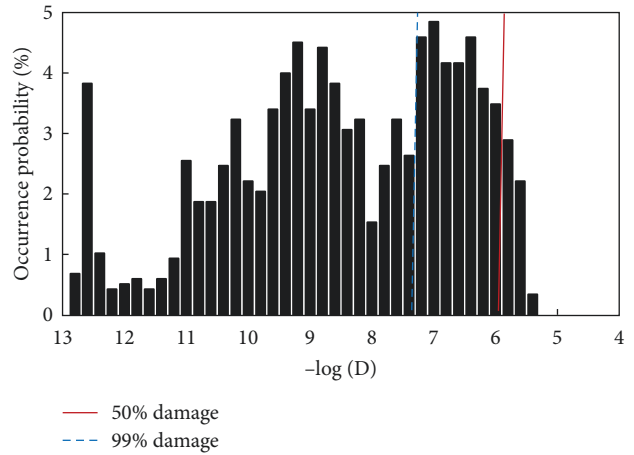


FIGURE 11: Occurrence probability of hourly fatigue damage.

obtained on the basis of fixed-point, linear extrapolation, and quadratic extrapolation methods are listed in Table 2.

5.2. Influence of Environment/Operation Conditions on Fatigue Damage. The strain time history during the monitoring period was transformed into the hot spot stress time history and hourly fatigue damage at the welded joint was calculated using the rainflow counting algorithm and the P–M damage accumulation rule to understand the influence of different operation conditions on fatigue damage. Figure 10 presents the hourly fatigue damage during the monitoring period (50 days, sampling frequency of 25 Hz). Points above the dotted blue line represent 99% of the total cumulated damage, while those above the solid red line account for 50% of the total cumulated damage. It can be seen that a few large wind speeds have a great influence on the fatigue damage of the structure.

Figure 11 illustrates the probability distribution of hourly fatigue damage. The peak value ($-\log(D) = 12.6$) on the left represents the hourly time series with nearly no damage. At this time, the wind turbine was in shutdown or standby states. The right side of the solid red line and the dotted blue line represent damage values greater than 50% and 99% of the total damage, respectively.

Figure 12 shows the percentage of hourly time series required to reach a certain damage level. The results demonstrated that 50% of the total damage was achieved within 5.02% of the monitoring time, and 99% of the total damage was achieved within 36.9% of the monitoring time. Therefore, it can significantly reduce the total fatigue damage and

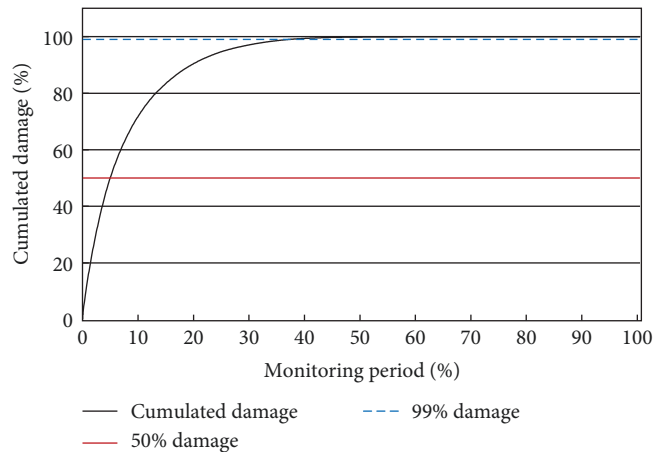


FIGURE 12: Percentage of cumulated damage over monitoring time.

retain sufficient power generation by detecting a few time periods that cause serious structural damage.

The damage mainly occurred during periods of high-wind speed. The influence of wind speed, rotation speed, and pitch angle on the hourly damage was also analyzed to examine the cause of this phenomenon (Figures 13–15). Points of the different colors in Figures 13–15 corresponding to the different operation states were summarized in Table 1.

Figure 13 shows that the hourly damage increased with the increase of wind speed. More than 50% of damage occurred between V_{rated} (11 m/s) and V_{cutout} (22 m/s). The corresponding $-\log(D)$ was 5.25–5.79, and the damage value range was $5.63E-6$ – $1.62E-6$. A very large number of hourly

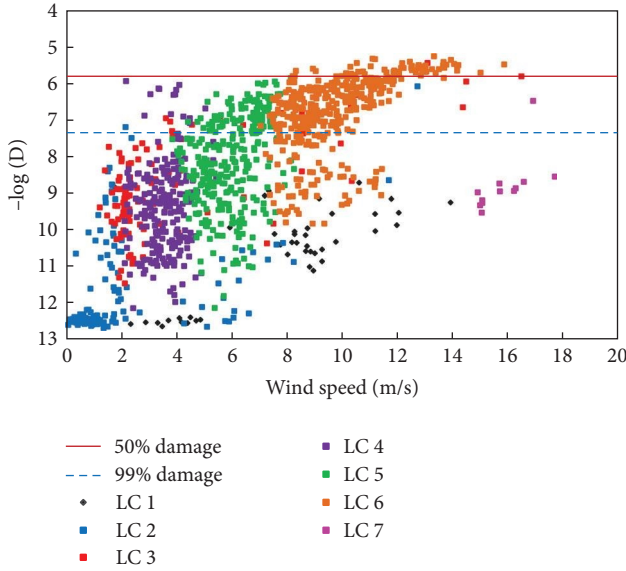


FIGURE 13: Relationship between hourly fatigue damage and wind speed.

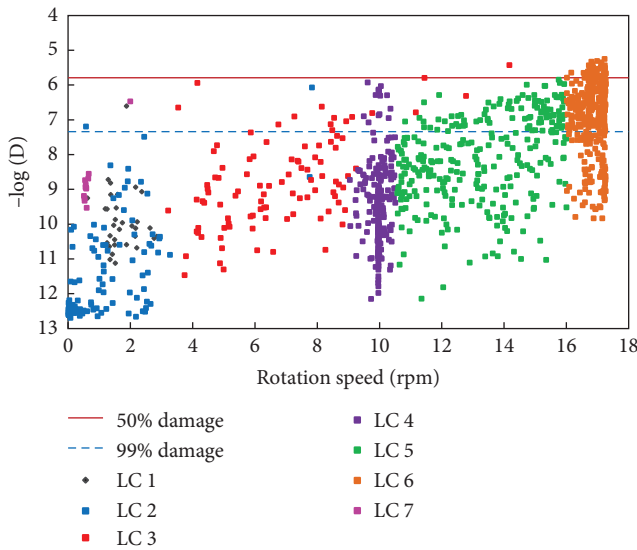


FIGURE 14: Relationship between hourly fatigue damage and rotation speed.

series was required to accumulate 1% of the total damage below the rated wind speed.

As shown in Figure 14, the damage increased with the increase of rotation speed. More than 50% of the total damage occurred near the rated rotation speed ($17.3 \text{ rpm} \pm 10\%$), and the corresponding wind speed was between V_{rated} and V_{cutout} (Figure 13). A small amount of large damage was caused by the transition conditions of startup and shutdown (red dot) states as well as emergency shutdowns (black dot) at high-wind speeds.

As shown in Figure 15, more than 50% of the damage occurred when the pitch control was active and the pitch angle changed from 0° to 20° , the corresponding wind speed was greater than V_{rated} . The pitch angle was constantly

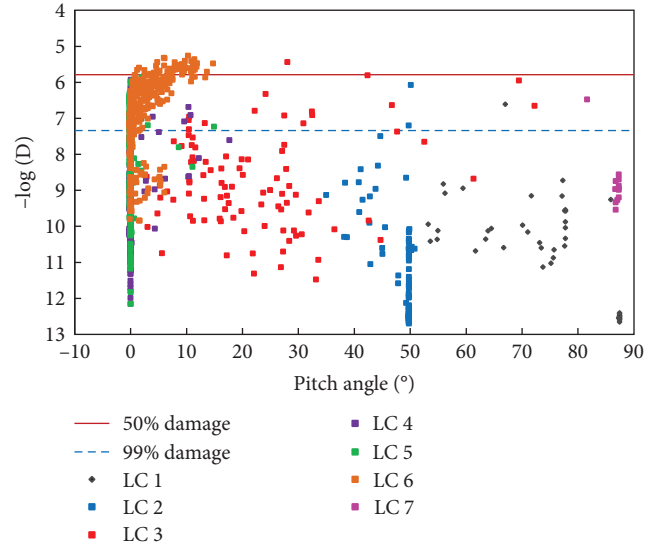


FIGURE 15: Relationship between hourly fatigue damage and pitch angle.

adjusted to maintain the rotation speed at the rated rotation speed and ensure maximum power output. Several red points above the dotted blue line with a pitch angle higher than 20° corresponded to the startup and shutdown processes of the wind turbine.

More than 50% of the damage occurred when the wind speed was greater than V_{rated} at rated rotation speed and the pitch control system varied from 0° to 20° . The rated wind speed state accounted for a small proportion of the monitoring period despite it being the main cause of fatigue damage. Emergency shutdowns and transition conditions of startup and shutdown were also periods of serious damage, but their probability of occurrence was very low and contribution to the damage was insignificant.

5.3. Fatigue Life Assessment Process. Strain data recorded continuously during the monitoring period can be used to establish a real stress spectrum, which can help to estimate the fatigue damage of the structure. If the monitoring period is more than 1 year, then strain data of the entire year can be selected for fatigue assessment. The wind speed and direction distribution in this time period is just the annual wind speed and direction distribution. However, if the monitoring period is less than 1 year, then the distribution of wind speed and direction cannot adequately represent the annual distribution of wind speed and direction. The direct use of data from this period for fatigue assessment will lead to inaccurate results. In this situation, structural damage can be estimated by correlating the annual wind speed and direction data from the SCADA system and the strain monitoring data of the wind turbine. The wind direction was divided into 12 regions, with the wind turbine as the center and $\theta = 30^\circ$ as an interval. The wind speed was divided into nine regions in each wind direction area. Therefore, the entire wind action plane was divided into 108 wind speed and direction combinations.

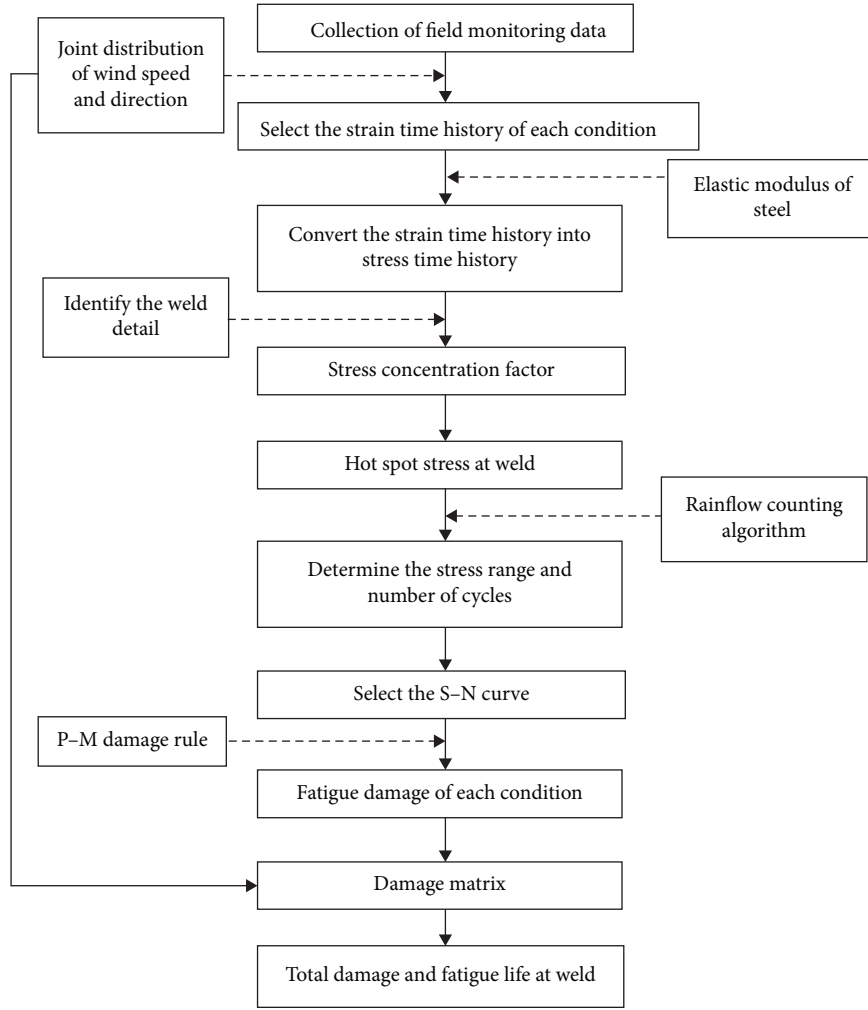


FIGURE 16: Fatigue life assessment process based on measured stress.

Figure 16 shows the process of fatigue life assessment based on short-term measured strain data and long-term SCADA data (minimum of 1 year). First, the strain time history corresponding to different combinations of wind speeds and directions was selected and transformed into stress time history. Second, the SCF at the flange weld was determined to obtain the hot spot stress time history at the weld. Finally, the hot spot stress time history was transformed into the stress spectrum using the rainflow counting algorithm, and the accumulated fatigue damage as well as the fatigue life at the weld were calculated using the P–M damage accumulation rule.

5.4. Damage Matrix. To calculate the fatigue damage in the entire service period using stress data of the monitoring period, the strain monitoring period should include all important operating states. In order to make the selected monitoring stress data in line with the joint distribution of annual wind speed and direction, it was necessary to calculate the damage under the different wind speeds and directions and stored it in the damage matrix:

$$[D_{u\theta}] = \begin{bmatrix} D_{11} & D_{12} & \cdots & D_{1\theta} \\ D_{21} & D_{22} & \cdots & D_{2\theta} \\ \vdots & \vdots & \vdots & \vdots \\ D_{u1} & D_{u2} & \cdots & D_{u\theta} \end{bmatrix}. \quad (8)$$

The occurrence probability of a certain wind speed level u is P_u and the occurrence probability of wind direction θ at wind speed level u is $Q_{u\theta}$ in time period T . The fatigue damage matrix of the structure component considering the joint distribution of wind speed and direction can be expressed using Equation (9):

$$[D_{u\theta}]_T = \begin{bmatrix} D_{11}P_1Q_{11} & D_{12}P_1Q_{12} & \cdots & D_{1\theta}P_1Q_{1\theta} \\ D_{21}P_2Q_{21} & D_{22}P_2Q_{22} & \cdots & D_{2\theta}P_2Q_{2\theta} \\ \vdots & \vdots & \vdots & \vdots \\ D_{u1}P_uQ_{u1} & D_{u2}P_uQ_{u2} & \cdots & D_{u\theta}P_uQ_{u\theta} \end{bmatrix}. \quad (9)$$

TABLE 3: Damage matrix corresponding to maximum hourly damage $[-\log(D)]$.

Wind direction	Wind speed (m/s)									D_{ave}
	0–3	3–5	5–7	7–9	9–11	11–13	13–15	15–17	17–19	
N	8.14	8.14	6.45	6.22	5.76	5.40	5.25	5.47	8.55	6.60
NNE	6.87	6.13	6.29	6.29	5.76	5.57	5.64	9.26	5.25	6.34
ENE	5.93	6.03	6.92	6.14	6.11	6.14	5.25	5.25	5.25	5.89
E	7.19	7.53	6.61	6.09	6.05	5.64	5.49	—	—	6.37
ESE	7.63	6.95	5.25	5.25	5.25	5.82	—	—	—	6.03
SSE	7.76	7.60	6.46	5.96	6.18	5.25	5.49	—	—	6.39
S	8.05	7.04	6.46	6.37	6.05	5.69	5.57	5.25	—	6.31
SSW	8.56	6.90	6.79	6.19	5.67	5.49	5.70	5.25	—	6.32
WSW	7.73	7.50	6.29	6.34	6.07	5.53	5.50	5.25	5.25	6.16
W	8.56	7.05	6.28	6.24	5.73	5.52	5.25	5.25	—	6.23
WNW	8.21	6.15	6.89	5.85	5.43	5.33	5.25	—	—	6.16
NNW	8.08	6.30	5.99	5.59	5.54	5.31	5.25	5.25	—	5.91
D_{ave}	7.73	6.94	6.39	6.04	5.80	5.56	5.42	5.78	6.08	

TABLE 4: Damage matrix corresponding to average hourly damage $[-\log(D)]$.

Wind direction	Wind speed (m/s)									D_{ave}
	0–3	3–5	5–7	7–9	9–11	11–13	13–15	15–17	17–19	
N	12.46	8.40	6.87	6.76	6.39	5.89	5.63	6.27	8.55	7.47
NNE	8.21	6.90	7.03	6.78	6.47	6.12	5.64	9.26	5.73	6.90
ENE	6.88	7.16	7.38	6.56	6.55	6.14	5.73	5.73	5.73	6.43
E	8.34	8.22	7.09	6.41	6.15	5.78	5.49	—	—	6.78
ESE	8.54	7.91	5.73	5.73	5.73	5.88	—	—	—	6.59
SSE	8.73	8.72	7.20	6.24	6.18	5.73	5.49	—	—	6.90
S	8.76	8.22	7.48	7.13	6.78	5.69	5.57	5.73	—	6.92
SSW	9.19	7.80	7.38	6.72	6.19	5.80	5.70	5.73	—	6.82
WSW	8.43	8.22	7.32	7.26	7.14	6.38	5.50	5.73	5.73	6.86
W	9.37	8.09	7.49	7.68	6.39	5.84	5.73	5.73	—	7.04
WNW	9.32	7.69	7.73	6.42	5.86	5.57	5.73	—	—	6.90
NNW	9.04	7.58	7.10	6.22	5.96	5.77	5.73	5.73	—	6.64
D_{ave}	8.94	7.91	7.15	6.66	6.32	5.88	5.63	6.24	6.44	

The total damage of the component in time period T can be obtained through the superposition of each term in the matrix as shown in Equation (10):

$$D_T = \sum_u \sum_{\theta} D_{u\theta} P_u Q_{u\theta}. \quad (10)$$

According to the P–M damage accumulation rule, the component will be damaged by fatigue when $D \geq \eta$. This (η) is the usage factor and $\eta = 1/\text{DFF}$, where DFF is the design fatigue factor [22].

Each wind speed and direction combination corresponded to several hourly damage values during the monitoring period. The maximum and average damage values were selected under the same wind speed and direction and then expressed with the negative logarithm $[-\log(D)]$, as shown in Tables 3 and 4. Among them, the fatigue life evaluated with average damage was closer to the actual value, while the maximum damage was conservative. The damage

increased with the increase of wind speed. The occurrence probability of some wind speed and direction combinations was 0 after a measuring period of more than 1 year because these combinations were absent during the monitoring period of the wind turbine.

The influence of the joint distribution of wind speed and direction on the fatigue damage was considered when the following were achieved. First, damage matrices calculated according to the maximum and average hourly damage $[-\log(D)]$ in Tables 3 and 4 were transformed into annual damage matrices. Second, the occurrence probability of different wind speeds and directions was multiplied to obtain the maximum and average annual total damage matrices under different combinations of wind speed and direction, as shown in Tables 5 and 6. Finally, the total annual damage at the flange weld was obtained by adding all the data in Tables 5 and 6.

5.5. Fatigue Life Assessment Results. The fatigue life of the flange weld of the wind turbine tower was analyzed using the

TABLE 5: Annual total damage matrix based on maximum hourly damage $[-\log(D)]$.

Wind direction	Wind speed (m/s)									D_{ave}
	0–3	3–5	5–7	7–9	9–11	11–13	13–15	15–17	17–19	
N	5.92	5.75	3.99	3.81	3.54	3.37	3.57	4.27	7.91	4.68
NNE	4.64	3.88	4.19	4.40	3.84	3.92	4.47	8.42	5.01	4.75
ENE	3.84	4.00	5.02	4.54	4.75	5.60	4.70	4.70	4.83	4.66
E	5.19	5.70	5.26	4.97	5.51	—	—	—	—	5.33
ESE	5.54	4.83	3.56	3.80	4.27	5.28	—	—	—	4.55
SSE	5.50	5.25	4.56	4.72	4.96	4.46	5.55	—	—	5.00
S	5.78	4.62	4.21	4.34	4.40	4.14	4.92	4.70	—	4.64
SSW	6.15	4.45	4.34	4.02	3.92	4.17	4.86	5.31	—	4.65
WSW	5.36	5.30	4.01	4.27	4.25	4.05	4.24	4.35	4.83	4.52
W	6.20	4.82	4.06	4.19	4.10	4.40	4.23	4.83	—	4.60
WNW	5.99	3.86	4.58	3.99	3.97	4.38	4.61	—	—	4.48
NNW	5.87	3.93	3.51	3.25	3.32	3.48	3.95	4.46	—	3.97
D_{ave}	5.50	4.70	4.27	4.19	4.24	4.29	4.51	5.13	5.64	

TABLE 6: Annual total damage matrix based on average hourly damage $[-\log(D)]$.

Wind direction	Wind speed (m/s)									D_{ave}
	0–3	3–5	5–7	7–9	9–11	11–13	13–15	15–17	17–19	
N	10.23	6.01	4.41	4.35	4.17	3.86	3.94	5.08	7.91	5.55
NNE	5.98	4.65	4.94	4.89	4.55	4.47	4.47	8.42	5.49	5.32
ENE	4.79	5.12	5.48	4.96	5.20	5.60	5.19	5.19	5.31	5.20
E	6.35	6.40	5.73	5.29	5.60	—	—	—	—	5.87
ESE	6.45	5.79	4.04	4.28	4.75	5.33	—	—	—	5.11
SSE	6.47	6.37	5.30	4.99	4.96	4.94	5.55	—	—	5.51
S	6.49	5.80	5.23	5.10	5.13	4.14	4.92	5.19	—	5.25
SSW	6.77	5.36	4.93	4.56	4.45	4.48	4.86	5.79	—	5.15
WSW	6.06	6.02	5.04	5.20	5.31	4.89	4.24	4.83	5.31	5.21
W	7.00	5.86	5.26	5.64	4.77	4.73	4.71	5.31	—	5.41
WNW	7.11	5.41	5.41	4.56	4.39	4.63	5.09	—	—	5.23
NNW	6.83	5.21	4.62	3.87	3.75	3.94	4.43	4.94	—	4.70
D_{ave}	6.71	5.67	5.03	4.81	4.75	4.64	4.74	5.59	6.00	

TABLE 7: Fatigue damage results of flange weld.

	Hourly mean damage	Hourly maximum damage
Annual total damage	1.88E-03	3.16E-03
Fatigue life (years)	266	158

strain data measured with a high-sampling frequency in 50 days and the joint distribution of wind speed and direction provided by SCADA system. The results are listed in Table 7. The calculated fatigue life was 266 years considering the hourly mean damage during the monitoring period and 158 years considering the hourly maximum damage.

The predicted fatigue life of the wind turbine tower based on measured strain was far greater than the design life of 20 years. This was because the fatigue damage and life calculated in the paper was based on the measured stress at 330° , which deviated approximately 10° from MWD and was not the location with the highest fatigue damage. Second, the strain monitoring time was relatively short, and some extreme

wind conditions may not have been recorded yet. Another important reason was that conservative assumptions were often used in wind turbine design to cover uncertainties in the environment, operation, and models. As a result, the effective fatigue load endured by the wind turbine was likely to be lower than the design assumptions provided by current codes, which will generate structural reserves [29]. Similar results were also obtained in Loraux's [17] study, where the predicted fatigue life of the tower based on strain monitoring was 165 years, which proved that the actual fatigue damage suffered by the wind turbine tower was relatively low compared to what could be expected from design. Hence, the service life of the wind turbine tower can be extended.

6. Conclusion

In this study, fatigue of a wind turbine tower is evaluated using measured strain data of the tower bottom and SCADA data of the wind turbine. The following conclusions can be drawn:

- (1) Operating states of the wind turbine were classified and the joint distribution probability of wind speed and direction was statistically analyzed according to SCADA data. The variation rule of stress at the tower bottom with average wind speed was calculated on the basis of measured strain data. The stress at the tower bottom first increased and then stabilized with the increase of wind speed, and it had great discreteness due to the influence of startup and shutdown of the rotor and yaw motion when the wind speed was lower than $V_{\text{cut-in}}$. Stress at the tower bottom reached the maximum value near V_{rated} and tended to stabilize when the wind speed was higher than V_{rated} .
- (2) The process of fatigue life assessment based on measured data was proposed. First, the SCF of the flange weld was calculated using the refined local finite element model, and the monitoring stress was transformed into the hot spot stress of the weld. Second, the rainflow counting algorithm and S–N curve were applied to calculate the hourly damage during the monitoring period. The maximum and mean annual total damage matrices were established according to the joint distribution of annual wind speed and direction. Finally, the total annual damage of flange weld were calculated using the P–M damage accumulation rule. The results indicated that fatigue life calculated using average (close to the actual value) and maximum (conservative estimation) values of the hourly damage during the monitoring period was 266 and 158 years, respectively. This finding shows that the wind turbine tower satisfies the requirement of 20 years design life.
- (3) The contribution of different operating conditions of the wind turbine to fatigue damage was quite different. Fatigue damage increased with the increase of wind and rotation speeds. More than 50% of the damage occurred when the wind speed was greater than V_{rated} with the rated rotation speed and the pitch control system varying from 0° to 20° .

Abbreviations

SCADA:	Supervisory control and data acquisition system
IEC:	International Electrotechnical Commission
DNVGL:	Det Norske Veritas and Germanischer Lloyd
IIW:	International Institute of Welding
S–N curve:	Stress (S) to fatigue life (N)
SCF:	Stress concentration factor
LC:	Load case
FA:	Fore–aft

RPM:	Revolutions per minute
DFE:	Design fatigue factor
MWD:	Main wind direction
SWD:	Secondary wind direction.

Symbols

$\Delta\sigma$:	Stress range
N :	Number of stress cycles to failure at stress range $\Delta\sigma$
m :	Negative inverse slope of S–N curve
$\log a$:	Intercept of S–N curve
t :	Thickness through which a crack will most likely grow
t_{ref} :	Reference thickness
k :	Thickness exponent on fatigue strength
σ_h :	Hot spot stress value at the weld toe
x_1, x_2, x_3 :	Extracting points at a certain distance from the weld toe
$\sigma_s(x_1), \sigma_s(x_2), \sigma_s(x_3)$:	Structural stress values at the extracting points x_1, x_2, x_3
$\Delta\sigma'$:	Effective stress range based on Goodman model
σ_m :	Mean stress
σ_t :	Ultimate tensile strength
i :	Total number of different stress levels
n_i :	Number of cycles accumulated at stress range $\Delta\sigma_i$
N_i :	Number of cycles to failure at stress range $\Delta\sigma_i$
D_i :	Fatigue damage component
D :	Accumulated fatigue damage
$V_{\text{cut-in}}$:	Cut-in wind speed
V_{cutout} :	Cutout wind speed
V_{rated} :	Rated wind speed
K_{SCF} :	Stress concentration factor
σ_h :	Hot spot stress
σ_r :	Reference stress
P_u :	Occurrence probability of wind speed u
$Q_{u\theta}$:	Occurrence probability of wind direction θ at wind speed u
η :	Usage factor
D_{ave} :	Average damage.

Data Availability

The data used to support the findings of this study are available from the first author upon request.

Conflicts of Interest

The authors declare that they have no conflicts of interest.

Acknowledgments

The authors gratefully acknowledge the financial support received from the National Natural Science Foundation of China

(51779224), Science and Technology Department of Henan Province of China (212102310978 and 222102320114).

References

- [1] J. D. Hua, "On the policy suggestion for promoting the development of wind energy resources in China," *Advanced Materials Research*, vol. 512–515, pp. 818–821, 2012.
- [2] M. P. Repetto and G. Solari, "Dynamic alongwind fatigue of slender vertical structures," *Engineering Structure*, vol. 23, no. 12, pp. 1622–1633, 2001.
- [3] M. P. Repetto and G. Solari, "Dynamic crosswind fatigue of slender vertical structures," *Wind and Structures*, vol. 5, no. 6, pp. 527–542, 2002.
- [4] M. P. Repetto and G. Solari, "Directional wind-induced fatigue of slender vertical structure," *Journal of Structural Engineering*, vol. 130, no. 7, pp. 1032–1040, 2004.
- [5] M. P. Repetto and G. Solari, "Bimodal alongwind fatigue of structures," *Journal of Structure Engineering*, vol. 132, no. 6, pp. 899–908, 2006.
- [6] J. V. D. Tempel, "Design of support structures for offshore wind turbines," Ph.D. thesis, Technische Universiteit Delft, Delft, Netherlands, 2006.
- [7] H. Bagbanci, D. Karmakar, and C. G. Soares, "Effect of the environment on the design loads on monopile offshore wind turbine," in *Maritime Engineering and Technology*, pp. 547–552, CRC Press, 1 edition, 2012.
- [8] M. I. Kvittem and T. Moan, "Time domain analysis procedures for fatigue assessment of a semi-submersible wind turbine," *Marine Structures*, vol. 40, pp. 38–59, 2015.
- [9] N. Stavridou, E. Efthymiou, and C. C. Baniotopoulos, "Welded connections of wind turbine towers under fatigue loading: finite element analysis and comparative study," *American Journal of Engineering and Applied Sciences*, vol. 8, no. 4, pp. 489–503, 2015.
- [10] Y. Edward Zhou, "Assessment of bridge remaining fatigue life through field strain measurement," *Journal of Bridge Engineering*, vol. 11, no. 6, pp. 737–744, 2006.
- [11] X. W. Ye, "Fatigue reliability assessment of steel bridges instrumented with structural health monitoring system," Ph.D. thesis, The Hong Kong Polytechnic University, Hong Kong, China, 2010.
- [12] X. W. Ye, Y. Q. Ni, and J. M. Ko, "Experimental evaluation of stress concentration factor of welded steel bridge T-joints," *Journal of Constructional Steel Research*, vol. 70, pp. 78–85, 2012.
- [13] T. H. T. Chan, Z. X. Li, and J. M. Ko, "Fatigue analysis and life prediction of bridges with structural health monitoring data—Part II: application," *International Journal of Fatigue*, vol. 23, no. 1, pp. 55–64, 2001.
- [14] E. A. Johnson, H. F. Lam, L. S. Katafygiotis, and J. L. Beck, "Phase I IASC-ASCE structural health monitoring benchmark problem using simulated data," *Journal of Engineering Mechanics*, vol. 130, no. 1, pp. 3–15, 2004.
- [15] M. C. Pollino and A. A. Huckelbridge, *In-situ Measurements of Fatigue Demands on a Wind Turbine Support Structure*, IEEE Energy Tech, Cleveland, USA, 2012.
- [16] W. Weijtens, N. Noppe, T. Verbelen, A. Iliopoulos, and C. Devriendt, "Offshore wind turbine foundation monitoring, extrapolating fatigue measurements from fleet leaders to the entire wind farm," *Journal of Physics: Conference Series*, vol. 753, no. 9, Article ID 092018, 2016.
- [17] C. T. Loraux, *Long-Term Monitoring of Existing Wind Turbine Towers and Fatigue Performance of UHPFRC under Compressive Stresse*, École Polytechnique Fédérale de Lausanne, Lausanne, Switzerland, 2018.
- [18] Q. A. Mai, W. Weijtens, C. Devriendt, P. G. Morato, P. Rigo, and J. D. Sørensen, "Prediction of remaining fatigue life of welded joints in wind turbine support structures considering strain measurement and a joint distribution of oceanographic data," *Marine Structures*, vol. 66, pp. 307–322, 2019.
- [19] Y. L. Xu, T. T. Liu, and W. S. Zhang, "Buffeting-induced fatigue damage assessment of a long suspension bridge," *International Journal of Fatigue*, vol. 31, no. 3, pp. 575–586, 2009.
- [20] Y. Q. Ni, X. W. Ye, and J. M. Ko, "Monitoring-based fatigue reliability assessment of steel bridges: analytical model and application," *Journal of Structural Engineering*, vol. 136, no. 12, pp. 1563–1573, 2010.
- [21] IEC 61400-1, *Wind Turbines-Part 1: Design Requirements*, IEC, Switzerland, 2005.
- [22] DNVGL-RP-C203, *Fatigue Design of Offshore Steel Structures*, DNV Recommended Practice, Norway, 2016.
- [23] X. L. Zhao and J. A. Packer, *Fatigue Design Procedure for Welded Hollow Section Joints*, Woodhead Publishing, 2000.
- [24] W. Fricke, "Recommended hot-spot analysis procedure for structural details of ships and FPSOs based on round-robin FE analyses," *International Journal of Offshore and Polar Engineering*, vol. 12, no. 1, pp. 40–47, 2002.
- [25] K. N. Smith, P. Watson, and T. H. Topper, "A stress-strain function for fatigue of metals," *Journal of Material*, vol. 5, no. 4, pp. 767–778, 1970.
- [26] Y. L. Lee, J. Pan, R. Hathaway, and M. Barkey, *Fatigue Testing and Analysis: Theory and Practice*, Elsevier Butterworth-Heinemann, 2004.
- [27] Y. Zhao, J. Pan, Z. Huang, Y. Miao, J. Jiang, and Z. Wang, "Analysis of vibration monitoring data of an onshore wind turbine under different operational conditions," *Engineering Structures*, vol. 205, Article ID 110071, 2020.
- [28] I. Losberg, "Fatigue design of plated structures using finite element analysis," *Ships Offshore Structures*, vol. 1, no. 1, pp. 45–54, 2006.
- [29] G. Marsh, "Fatigue load monitoring of offshore wind turbine support structures," Ph.D. thesis, University of Strathclyde, Glasgow, Scotland, 2016.